Can Zn isotopes in sediments record past eutrophication of freshwater lakes ? A pilot study at Lake Baldegg (Switzerland)

F. Juillot[1,2], V. Noël[1,3], A. Gelabert[4], D. Jouvin[4], P. Louvat[4], J. Göttlicher[5], S. Belin[6], B. Mueller[7], G. Morin[1] and A. Voegelin[8]

[1]Institut de Mineralogie, de Physique des Materiaux et de Cosmochimie, IMPMC, Sorbonne Universite, UMR CNRS 7590, MNHN, ERL IRD 206, 4 Place Jussieu, 75005 Paris, France

[2]Institut de Recherche pour le Developpement, IRD, Centre NOUMEA, 101 Promenade Roger Laroque, 98848 Noumea Cedex, New Caledonia

[3]Stanford Synchrotron Radiation Laboratory, SLAC National Accelerator Laboratory, 2575 Sand Hill road, Menlo Park, CA 94025, California, USA

[4]Institut de Physique du Globe de Paris, IPGP, UMR CNRS 7154, 1 rue Jussieu, 75238 Paris cedex 05, France

[5]Karlsruhe Institute of Technology, Institute for Photon Science and Synchrotron Radiation, KIT Campus North, Hermann-von-Helmholtz-Platz 1, D-76344 Eggenstein-Leopoldshafen, Germany

[6]Synchrotron SOLEIL, SAMBA beamline, L'Orme des Merisiers, 91190 Saint-Aubin, France

[7]Eawag, Swiss Federal Institute of Aquatic Science and Technology, Seestrasse 79, 6047 Kastanienbaum, Switzerland

[8]Eawag, Swiss Federal Institute of Aquatic Science and Technology, Überlandstrasse 133, 8600 Dübendorf, Switzerland

SUPPLEMENTARY MATERIAL

1. Quality of Zn isotope data

The quality of the Zn isotope data used in this study was checked by plotting all measured $\delta^{68}Zn$ values as a function of the corresponding $\delta^{66}Zn$ values. On such a diagram, Zn isotope data should follow a linear relationship if they result from mass dependent fractionation and instrumental mass bias have been well corrected. For a diagram depicting $\delta^{68}Zn$ *vs.* $\delta^{66}Zn$ values, the slope of the kinetic mass dependent fractionation line should be 1.94 (Maréchal et al., 1999).

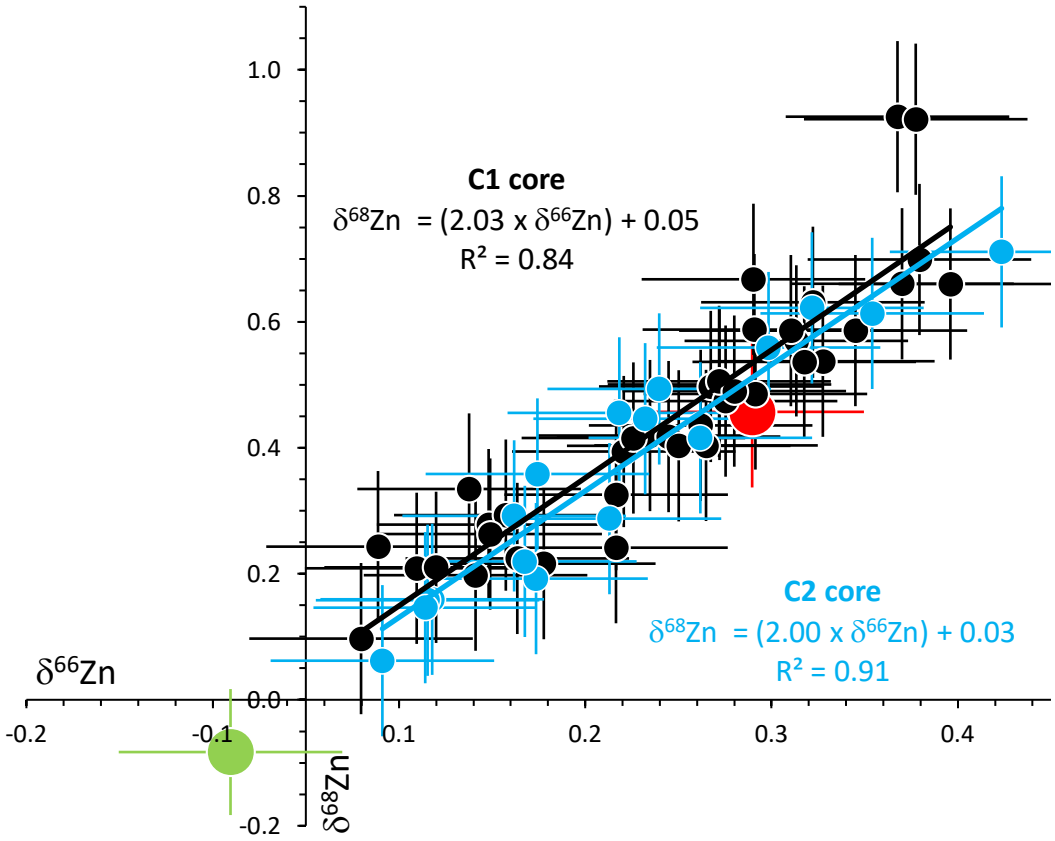

Figure S1. $\delta^{68}Zn$ vs. $\delta^{66}Zn$ diagram for all the samples from core 1 (black) and core 2 (blue) analyzed during this study. The average $\delta^{68}Zn$ and $\delta^{66}Zn$ values for the JMC-Lyon (green) and IRMM (red) standards are also shown. The slope of the regression line across each dataset (*i.e.* 2.03 for core 1 and 2.00 for core 2, compared to the expected theoretical value of 1.94) and the good related correlation coefficients (*i.e.* R^2 = 0.84 for core 1 and 0.91 for core 2) emphasize the reliability of the Zn isotope analyses.

Despite two outliers from core 1, the diagram displayed in Figure S1 (corresponding data in Tables S1 and S2) shows a good alignment of the Zn isotopes data (*i.e.* R^2 = 0.84 and 0.91 for core 1 and core 2, respectively), with a slope (*i.e.* 2.03 and 2.00 for core 1 and core 2, respectively) close to the expected theoretical one (*i.e.* 1.94). These values emphasize the good quality of the Zn isotope data used in this study.

Table S1. δ^{66}Zn and δ^{68}Zn values of the two standards (JMC-Lyon and IRMM) used for this study. The uncertainty estimated at the 95% confidence level for both standards is 0.03‰ (2σ = 0.06‰) on δ^{66}Zn and 0.06‰ (2σ = 0.12‰) on δ^{68}Zn.

	δ^{66}Zn	δ^{68}Zn		δ^{66}Zn	δ^{68}Zn
JMC-Lyon	-0.02	-0.02	mean	-0.04	-0.08
	-0.02	-0.06	sd	0.03	0.05
	-0.05	-0.14			
	-0.02	-0.05			
	-0.09	-0.14			
IRMM	0.24	0.39	mean	0.24	0.46
	0.29	0.60	sd	0.03	0.06
	0.25	0.53			
	0.29	0.52			
	0.22	0.30			
	0.28	0.54			
	0.19	0.44			
	0.20	0.44			
	0.16	0.36			
	0.23	0.46			
	0.24	0.49			
	0.23	0.45			
	0.25	0.46			
	0.24	0.45			
	0.23	0.43			
	0.23	0.42			
	0.24	0.43			
	0.26	0.45			
	0.23	0.44			
	0.24	0.46			
	0.27	0.50			
	0.26	0.49			

Table S2. $\delta^{66}Zn$ and $\delta^{68}Zn$ values of all sediments analyzed from core 1, including white and black varves isolated from few selected samples. The two samples in red show slight deviation from the linear correlation reported in Figure S1.

Depth (cm)	$\delta^{66}Zn$	$\delta^{68}Zn$	
4.5	0.04	0.24	
7.5	0.09	0.20	
10.5	0.06	0.21	
10.5 bv	0.09	0.33	black varves
10.5 bv	0.10	0.28	black varves
10.5 bv	0.11	0.29	black varves
10.5 wv	0.17	0.33	white varves
13.5	0.03	0.10	
16.5	0.10	0.26	
19.5	0.07	0.21	
22.5 bv	0.11	0.22	black varves
22.5 bv	0.13	0.22	black varves
22.5 bv	0.17	0.24	black varves
22.5 wv	0.18	0.42	white varves
22.5 wv	0.17	0.39	white varves
22.5 wv	0.24	0.49	white varves
22.5 wv	0.18	0.42	white varves
25.5	0.19	0.42	
28.5 bv	0.22	0.50	black varves
28.5 wv	0.24	0.59	white varves
28.5 wv	0.28	0.54	white varves
28.5 wv	0.22	0.50	white varves
31.5	0.21	0.44	
34.5	0.23	0.47	
34.5 bv	0.26	0.57	black varves
34.5 bv	0.32	0.66	black varves
34.5 bv	0.33	0.70	black varves
34.5 wv	0.32	0.93	white varves
34.5 wv	0.33	0.92	white varves
37.5	0.22	0.51	
37.5	0.21	0.40	
37.5	0.20	0.40	
40.5	0.27	0.63	
40.5	0.27	0.54	
43.5	0.35	0.66	
43.5	0.30	0.59	
43.5 cf	0.23	0.49	Clay fraction
46.5	0.24	0.67	

49.5	0.26	0.59

Depth (cm)	δ^{66}Zn	δ^{68}Zn
1.5	0.11	0.16
4.5	0.19	0.36
4.5	0.14	0.33
10.5	0.10	0.23
10.5	0.16	0.27
10.5	0.10	0.19
10.5	0.08	0.14
19.5	0.16	0.30
31.5	0.16	0.44
31.5	0.23	0.57
31.5	0.25	0.50
31.5	0.22	0.53
43.5	0.41	0.79
43.5	0.37	0.58
46.5	0.21	0.54
46.5	0.29	0.64
46.5	0.30	0.83
46.5	0.34	0.69
46.5	0.31	0.70

Table S3. δ^{66}Zn and δ^{68}Zn values of all sediments analyzed from core 2.

2. Mineralogical characteristics of the sediments

The XRD patterns of all the samples collected along the studied sediment core are displayed in Figure S2. Since calcite was the most abundant mineral in all samples, the XRD powder patterns were normalized to the intensity of the main *(104)* peak of this mineral species to allow qualitative comparison from one to another.

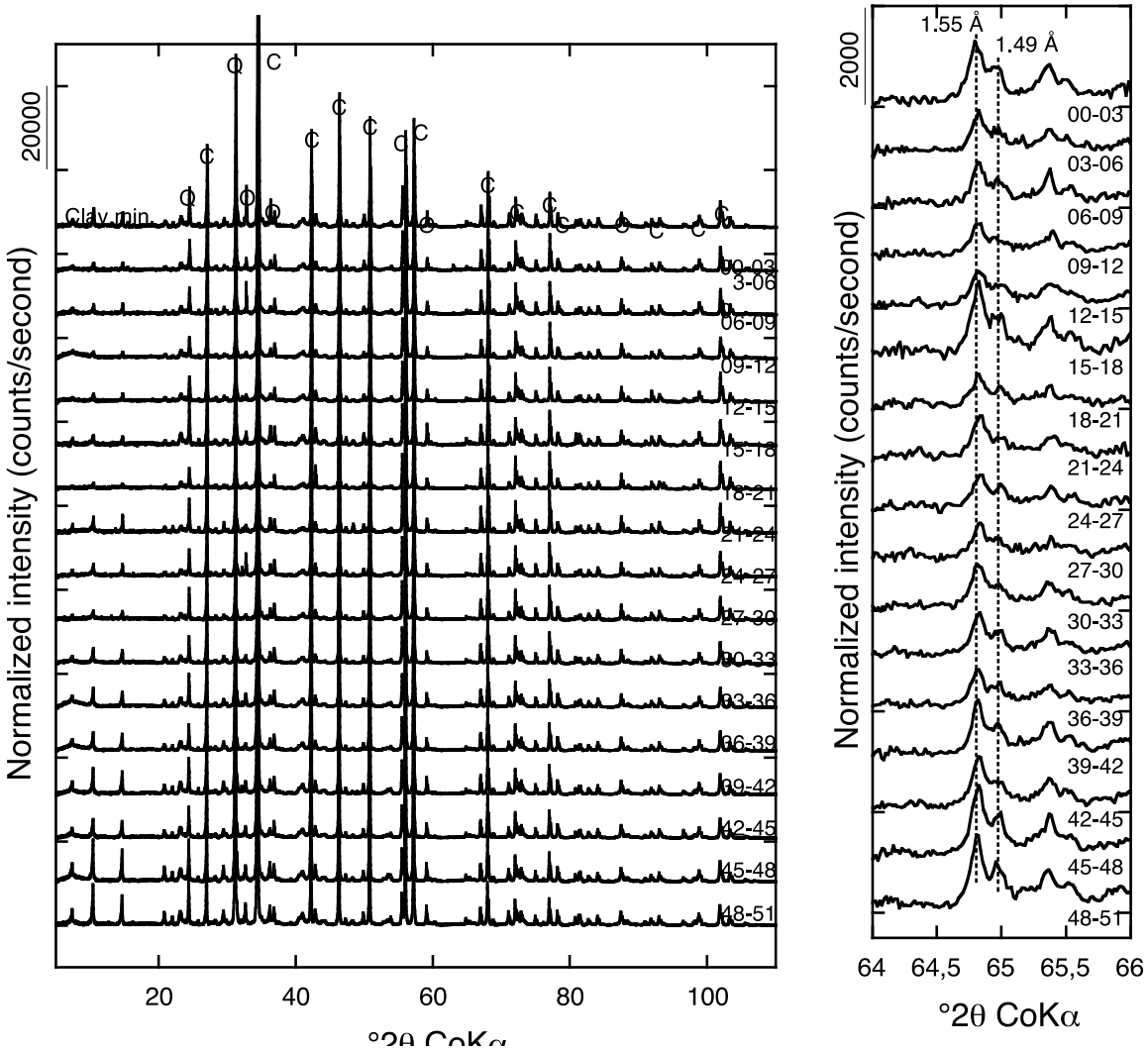

Figure S2. Whole powder X-ray diffraction patterns (left) and zoomed view in the 64-66 °2θ range (right) of samples collected with 3 cm depth intervals across the sediments at Lake Baldegg. C: Calcite. Clay min.: Clay minerals (identified in Figure S2). O: Orthoclase. Q: Quartz.

The origin (autochthonous *vs.* allochthonous) of the clay minerals can be qualitatively assessed from this figure through simple evaluation of their weight fraction relative to that of biochemical calcite. At a first order, this evaluation can be provided by the visual inspection of the intensity of the XRD peaks at 2θ angles below 20° on the XRD powder patterns. Although possible preferred orientation effects due to the anisotropic character of the clay minerals could induce some bias in this procedure by modifying the intensity of their *(00l)* XRD peaks (Brindley and Brown. 1980), these possible effects are likely minor since all oriented mounts were prepared following the same protocol. The

intensity of the *(00l)* XRD peaks of clay minerals on the calcite-normalized XRD powder patterns can thus be considered to reflect the actual weight fraction of the clay minerals with respect to calcite in the analyzed samples. Visual inspection of the calcite-normalized XRD powder patterns indicates that the strongest intensity for the *(00l)* XRD peaks of clay minerals is found in bottom samples, and to a lesser extent in the two topmost samples (Figure S2). The estimated weight fraction of the clay minerals appears thus larger during the pre-eutrophic period (bottom samples) and after lake restoration (surface samples) when allochthonous sedimentation prevailed. Such an evolution supports the allochthonous origin of the clay minerals identified in the sediments from Lake Baldegg. Actual nature of the clay minerals in the sediments from Lake Baldegg was assessed by a detailed analysis of the XRD patterns collected on oriented mounts of the clay fractions separated from selected samples (*i.e.* 3-6 cm, 21-24 cm, 33-36 cm and 45-48 cm depths; Figure S3). For all samples, the XRD patterns of the air-dried clay fractions show a first large peak centered around 7.2 °2θ that can be attributed to 14 Å phyllosilicates (chlorite and/or vermiculite and/or smectite), a second sharper peak at 10.1 °2θ that can be attributed to illite and a third peak at 14.3 °2θ that can be attributed either to the *(001)* reflection of kaolinite or to the *(002)* reflection of the 14 Å phyllosilicates (Figure S3). Upon heating at 250°C and 500°C. the large peak around 7.2 °2θ strongly decreases and only a small peak remains (Figure S3), which emphasizes the occurrence of chlorite. In addition, the intensity of the peak at 14.3 °2θ significantly decreases from the air-dried patterns to those heated at 500°C, which indicates a contribution of the *(001)* reflection of kaolinite. However, the persistence of this peak at 14.3 °2θ after heating at 500°C during one hour also indicates a contribution of the *(002)* reflection of chlorite. Finally, upon ethylene-glycol solvation, the large peak around 7.2 °2θ shifts towards smaller angles with a maximum around 6.0 °2θ, which is related to the occurrence of smectite. The small residual peak at 7.2 °2θ that remains after ethylene-glycol solvation is related to the occurrence of chlorite. These results indicate that the clay fraction of the studied sediments is mainly composed of smectite and illite, and to a lesser extent of kaolinite and chlorite. Such a mixture of dioctahedral and trioctahedral phyllosilicates is in agreement with the two *(060)* peaks around 65°

2θ (*i.e.* d-spacing of 1.49 Å and 1.55 Å) that can be seen on the bulk XRD powder patterns of the selected samples displayed in Figure S2 (Brindley and Brown. 1980).

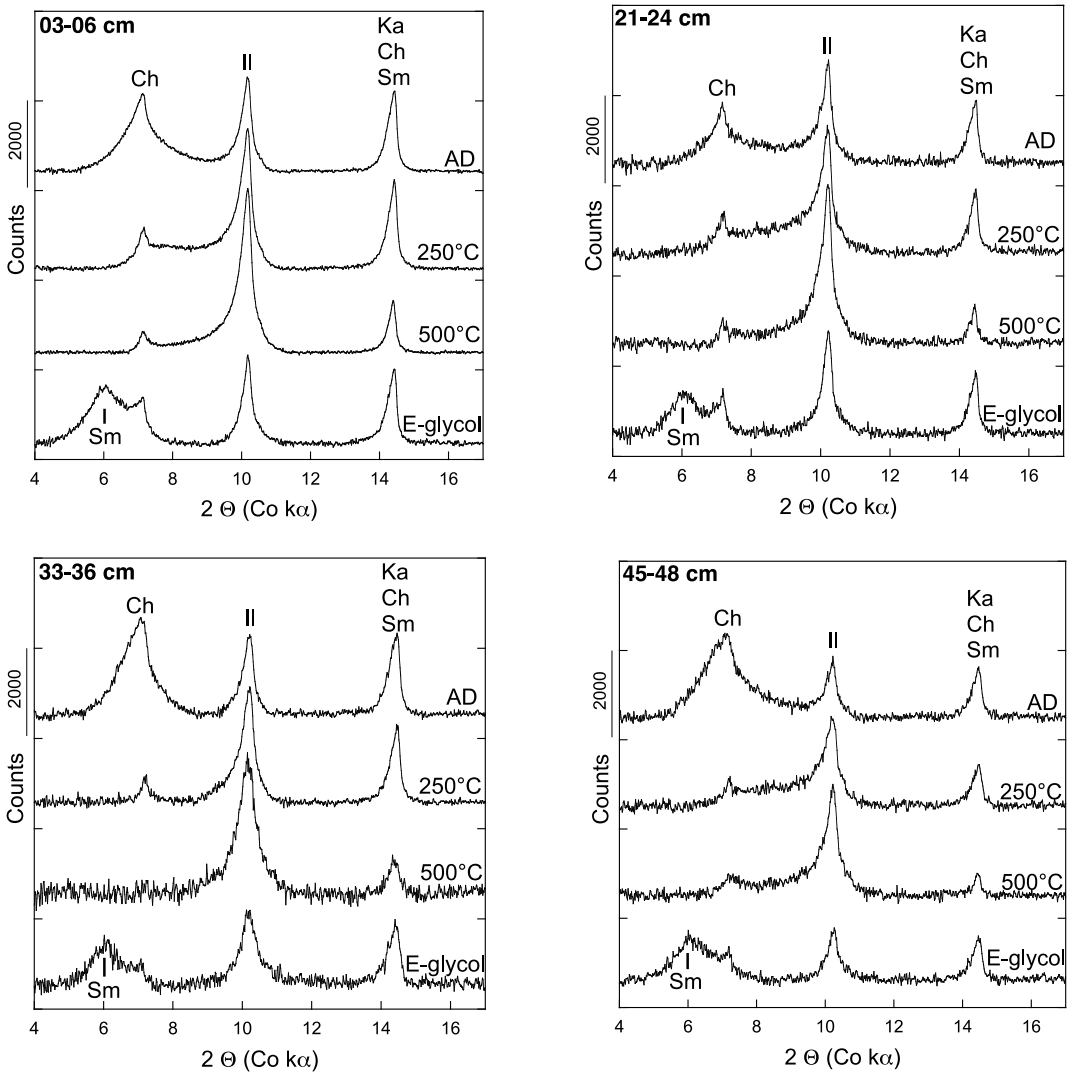

Figure S3. Zoomed view in the 4-17 °2θ range of the X-ray diffraction patterns collected on oriented mounts of clay fraction (< 2 µm) of selected samples from various depths across sediments at Lake Baldegg. AD : Air dried. E-glycol : Treated with Ethylene Glycol. 250°C : Heated at 250°C during 1 hour. 500°C : Heated at 500°C during 1 hour. Ch : Chlorite. Il : Illite. Ka: Kaolinite. Sm : Smectite.

3. Chemical characteristics of the sediments

Despite a shift of about 15 mg/kg, the vertical evolution of the Zn concentration estimated by XRF at Eawag (Switzerland) on core 1 and the Zn concentration estimated by XRF at IMPMC (France) on core 2 appear similar (Figure S4. left; Table S4). This is confirmed by the correlation plot between both Zn concentration datasets (Figure S4. right).

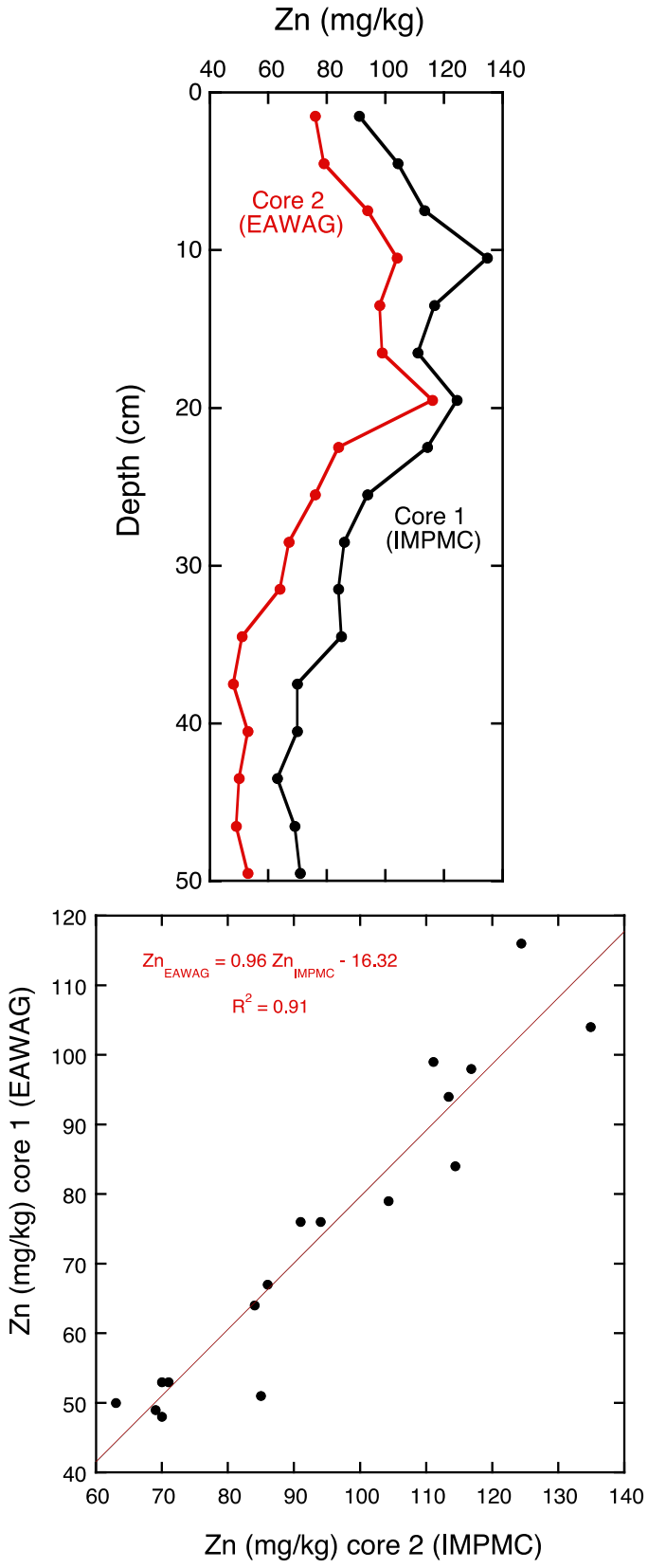

Figure S4. (left) Vertical evolution of the Zn concentration estimated by XRF at Eawag (Switzerland) on core 1 and the Zn concentration estimated by XRF at IMPMC (France) on

core 2. (right) Correlation between the Zn concentration estimated by XRF at Eawag on core 1 and the Zn concentration estimated by XRF at IMPMC on core 2.

Table S4. Vertical evolution of the Zn concentration estimated by XRF at Eawag (Switzerland) on core 1 and the Zn concentration estimated by XRF at IMPMC (France) on core 2.

Sample	Zn core 1 (EAWAG) (mg/kg)	Zn core 2 (IMPMC) (mg/kg)
1.5	76	91
4.5	79	104
7.5	94	113
10.5	104	135
13.5	98	117
16.5	99	111
19.5	116	124
22.5	84	114
25.5	76	94
28.5	67	86
31.5	64	84
34.5	51	85
37.5	48	70
40.5	53	70
43.5	50	63
46.5	49	69
49.5	53	71

The Zn concentration profile across core 2 is similar to that of S (*i.e.* associated with sulfides) and Ca (*i.e.* associated with calcite) and opposite to that of Al and K (*i.e.* associated with orthoclase and clay minerals; Figures 2 and S5).

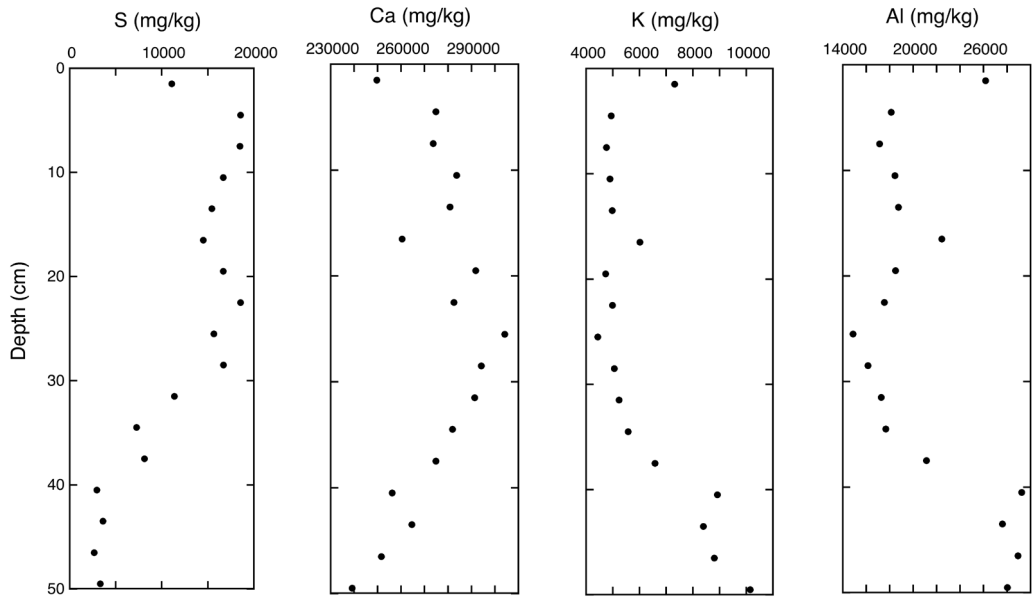

Figure S5. Bulk concentration (mg/kg) profiles of S, Ca, K and Al averaged across cores 1 and 2.

After analysis of the normal distribution of the data by a Shapiro-Wilk test, a Spearman test was performed on the Zn, K, Ca, Al and S concentrations in order to depict the statistical correlations between elements across core 2. The Spearman correlation coefficients retrieved at a 5% confidence level (p-value < 0.05) indicated positive correlations between Zn and S (0.83***) and Al and K (0.95***), and negative correlations between, Ca and K (-0.86***), Ca and Al (-0.89***), S and K (-0.89***) and S and Al (-0.82***) (Table S5).

Table S5. Pearson correlation coefficients between bulk Zn, K, Ca, Al and Zn concentration averaged across sediments cores 1 and 2.

	Zn	K	Ca	Al	S
Zn	--	-0.71**	0.41	-0.56*	**0.83*** **
K	--	--	**-0.86*** **	**0.95*** **	**-0.89*** **
Ca	--	--	--	**-0.89*** **	0.64**
Al	--	--	--	--	**-0.82*** **
S	--	--	--	--	--

***p-value < 0.01.

4. Chemometric grouping of the sediments

The sediments from cores 1 and 2 were grouped according to a Hierarchical Cluster Analysis (HCA), an unsupervised iterative classification, which consists in forming groups by progressive agglomeration of pairwise closest individuals. For that purpose, the Ward's criterion and the Euclidean distance were respectively used as the agglomeration method and as a measure of the similarities between the individuals. The HCA was performed on the sediments from cores 1 and 2 by considering Zn, Ca, Al, K and S averaged concentrations. The HCA results shown in Figure S6 as dendrograms indicate that the sediments collected below 37.5 cm depth (*i.e.* in the non-varved section characteristic of the pre-eutrophic period) fall in a first group, whereas those collected between 37.5 cm and 25.5 cm depth (*i.e.* lower half of the varved section characteristic of the eutrophic period) fall in a second group and the sediments collected between 25.5 cm depth and 7.5 cm depth (*i.e.* upper half of the varved section characteristic of the eutrophic period) fall in a third group, and the two uppermost sediments (*i.e.,* deposited after lake restoration) fall in a fourth group.

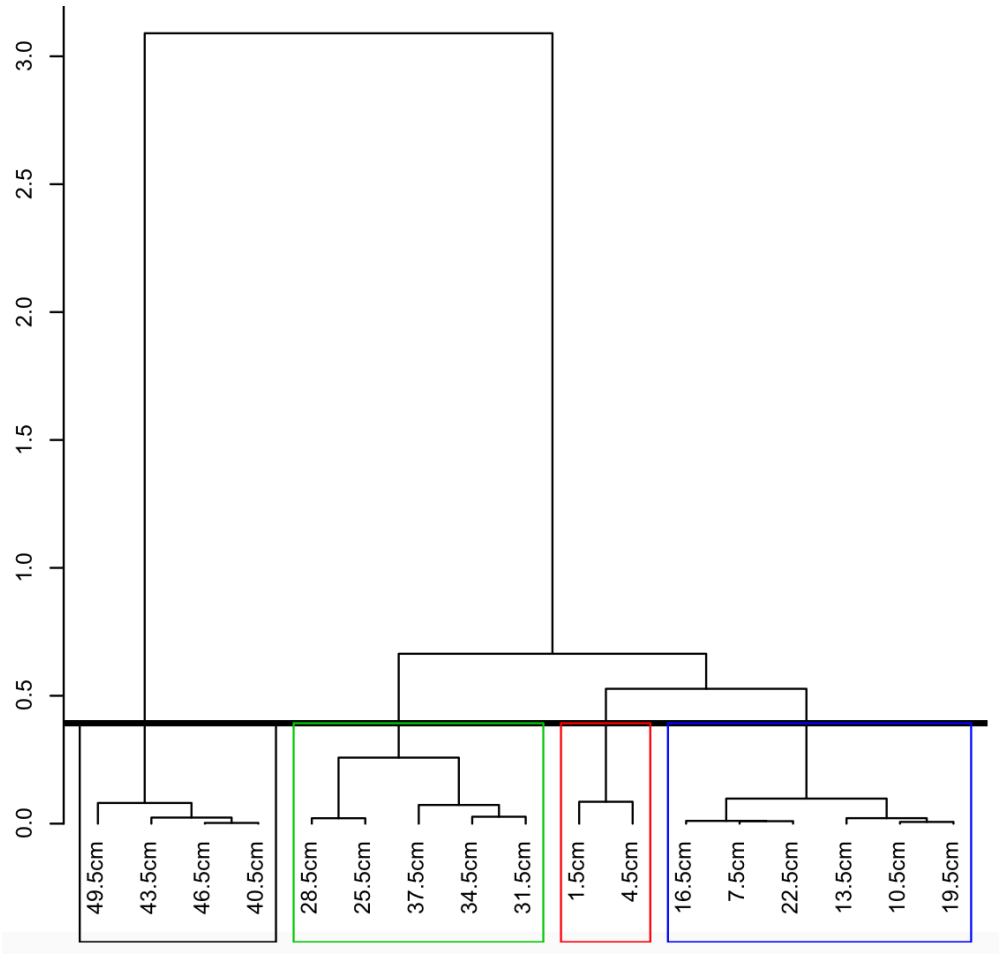

Figure S6. Results of a Hierarchical Cluster Analysis (HCA) performed on the sediments of Lake Baldegg by considering the Zn, Ca, Al, K and S concentration averaged from cores 1 and 2. Four groups are separated: the non-varved sediments collected below 37.5 cm depth (black frame), the lower-half section of the varved sediments collected between 37.5 and 25.5 cm depth (green frame), the upper-half section of the varved sediments collected between 25.5 and 7.5 cm depth (blue frame) and the non-varved sediments collected above 4.5 cm depth (red frame).

5. Linear regression between Zn isotope and speciation data

The linear regression between Zn isotope and speciation data across the sediments of Baldegg (Tables 1 and 2) depicted in Figure 3 showed a significant correlation ($R^2 = 0.57$, p-value < 0.01, n = 12). However, it also showed that the sample collected at 1.5 cm depth (*i.e.*, $\delta^{66}Zn = +0.04$ and Zn as ZnS = 0.46; Tables 1 and 2) was out of the regression line. A second linear regression was thus passed across the same dataset after removing this sample. This new linear regression yielded a better correlation ($R^2 = 0.69$, p-value < 0.01, n = 11; Figure S7) and the $\delta^{66}Zn$ values derived for the Zn-clays pool (*i.e.,* +0.29‰ ±0.04‰) and the ZnS pool (*i.e.,* 0.00‰ ±0.06‰) were similar to those retrieved from the linear regression across the complete dataset (*i.e.,* +0.27‰ ±0.05‰ and 0.00‰ ±0.08‰, respectively; Figure 3).

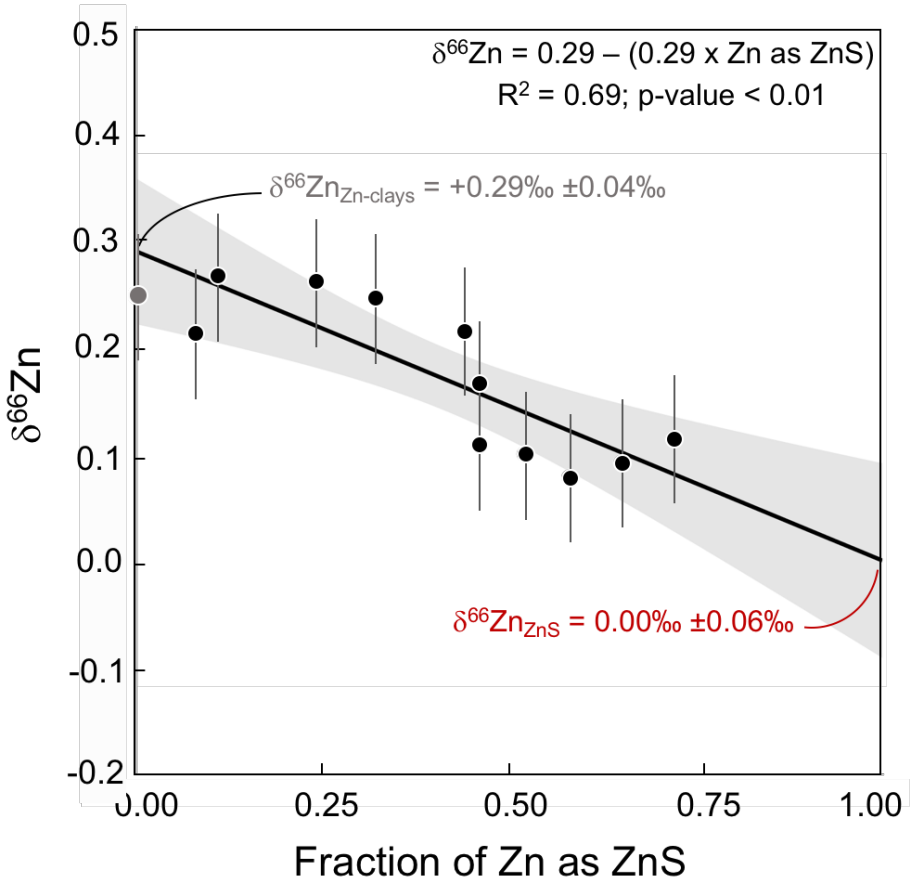

Figure S7. Linear regression between the $\delta^{66}Zn$ values and the fraction of Zn quantified as ZnS by XANES spectroscopy across the sediments of Lake Baldegg, after removing the sample collected at 1.5 cm depth that stands out of the regression line when all available data are considered (Figure 3). The gray point corresponds to the clay fraction separated from the sample collected at 43.5 cm depth.The gray area corresponds to the 95% confidence interval of the regression line.

6. Linear regression between Zn isotope and reverse Zn concentration

The progressive trend of $\delta^{66}Zn$ values across the sediments of Baldegg was further attested for by the linear regression that could be depicted between Zn isotope and the reverse Zn concentration measured across all the samples (Table 1) with a good correlation ($R^2 = 0.80$, p-value < 0.01, n = 17; Figure S8).

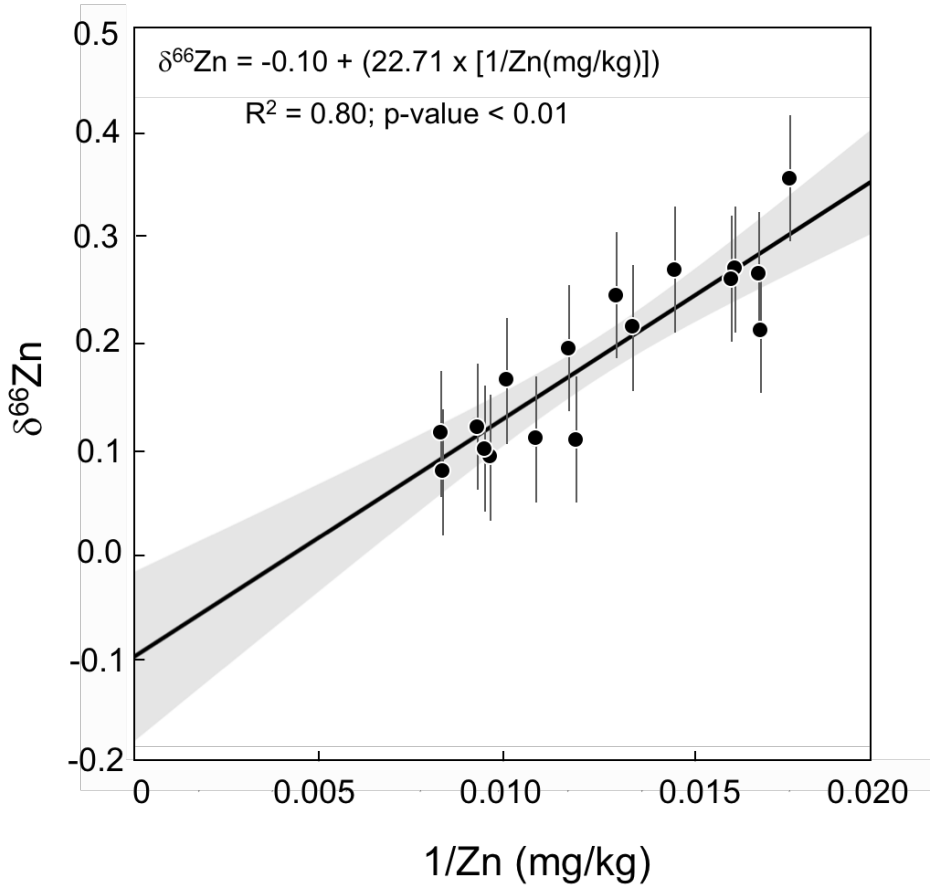

Figure S8. Linear regression between the $\delta^{66}Zn$ values and the reverse of the Zn concentration measured across the sediments of Baldegg (Table 1). The gray area corresponds to the 95% confidence interval of the regression line.

7. Linear regression between Zn isotope and total organic carbon content in white and black varves separated from selected eutrophic sediments

Linear regression between the $\delta^{66}Zn$ values and the reverse of the total organic carbon contents quantified in white and black varves separated from selected eutrophic sediments (*i.e.*, 10.5 cm depth, 22.5 cm depth, 28.5 cm depth and 34.5 cm depth; Figure 2; Table 1) showed a very good correlation ($R^2 = 0.90$, p-value < 0.01, n = 8; Figure S9).

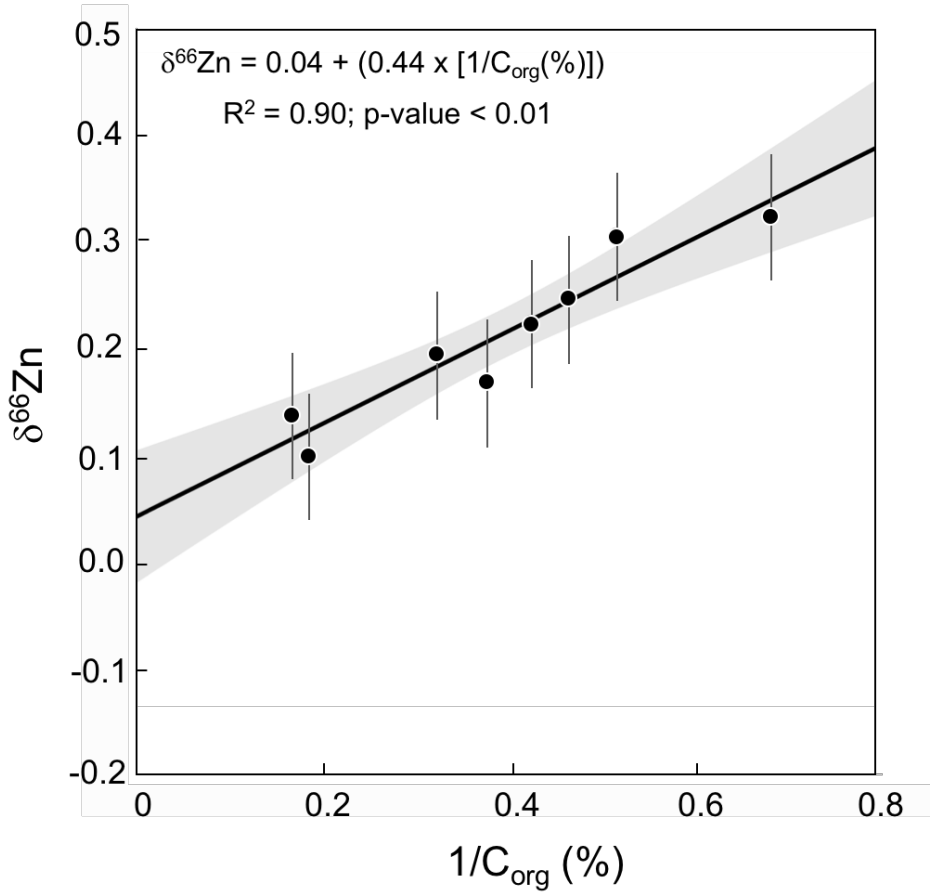

Figure S9. Linear regression between the $\delta^{66}Zn$ values and the reverse of the total organic carbon content measured in black and white varves separated from selected eutrophic sediments (Figure 2; Table 1). The gray area corresponds to the 95% confidence interval of the regression line.

References

Brenner M., Whitmore T.J., Curtis J.H., Hodell D.A. and Schelske C.L. (1999) Stable isotope (δ13C and δ15N) signatures of sedimented organic matter as indicators of historic lake trophic state. *J. Paleolimnol*., **22**, 205–221.

Brindley G.W. and Brown G. (1980) Crystal structures of Clay Minerals and Their Identification. Mineralogical Society Monograph N° 5. Mineralogical Society. London.

Hodell D.A. and Schelske C.L. (1998) Production, sedimentation and isotopic composition of organic matter in Lake Ontario. *Limnol. Oceanogr.,* **43**, 200–214.

Maréchal C.N., Telouk P. and Albarede F. (1999) Precise analysis of copper and zinc isotopic compositions by plasma-source mass spectrometry. *Chem. Geol.,* **156**, 251–273.

Neumann T., Sstögbauer A., Walpersdorf E., Stüben D. and Kunzendorf H. (2002) Stable isotope in recent sediment of Lake Arendsee NE Germany: Response to eutrophication and remediation measures. *Paleogeo. Palaeoclim. Palaeoecol.,* **178**, 75–90.

Teranes J.L., Mckenzie J.A., Bernasconi S.M., Lotter A.F. and Sturm M. (1999*)* Stable isotope response to lake eutrophication: Calibration of a high-resolution lacustrine sequence from Baldeggersee, Switzerland. *Limnol. Oceanogr.,* **44**, 320–333.

Teranes J.L. and Bernasconi S.M. (2005) Factors controlling $\delta^{13}C$ values of sedimentary carbon in hypertrophic Baldeggersee, Switzerland, and implications for interpreting isotope excursions in lake sedimentary records. *Limnol. Oceanogr.,* **50**, 914–922.